

The effects of Higgs boson couplings through HZZ production at future lepton colliders

S. Spor^{1,*}

¹*Department of Medical Imaging Techniques,
Zonguldak Bülent Ecevit University, 67100, Zonguldak, Türkiye.*

Abstract

We focus on the sensitivity of the Higgs-gauge boson couplings at $H\gamma Z$ and HZZ vertices through the process $\ell^-\ell^+ \rightarrow HZZ$ at CLIC and Muon Collider. Signal and relevant background events are generated in MadGraph within Standard Model Effective Field Theory (SMEFT) framework. These events are passed through Pythia for parton showering, and realistic detector effects are simulated by Delphes. The limits at 95% C.L. on the coefficients \bar{c}_{HB} and \bar{c}_{HW} are obtained at three b-tagging working points; loose, medium, and tight containing the Delphes card from CLIC and Muon Collider, corresponding to b-tagging efficiencies of 90%, 70%, and 50%, respectively. We report that our best 95% C.L. limits on \bar{c}_{HB} and \bar{c}_{HW} coefficients are $[-0.00098; 0.00047]$ and $[-0.00158; 0.00008]$, respectively, at 3 TeV CLIC with an integrated luminosity of 5 ab^{-1} , and $[-0.00021; 0.00019]$ and $[-0.00019; 0.00007]$, respectively, at 10 TeV Muon Collider with an integrated luminosity of 10 ab^{-1} . These limits are compared with the present experimental and various phenomenological limits.

*serdar.spor@beun.edu.tr

I. INTRODUCTION

The discovery of the Higgs boson by the ATLAS [1] and CMS [2] collaborations at the Large Hadron Collider (LHC) has been a fundamental milestone in confirming the electroweak symmetry breaking mechanism predicted by the Standard Model (SM). Although the SM is largely consistent with experimental measurements to date, it cannot answer many fundamental questions. This suggests that new physics effects may arise beyond the SM, making precise investigation of the Higgs boson's interactions particularly important. The deviations in the measured properties of the Higgs boson may be indirect indicators of new physics scenarios that are not yet directly observable. In this context, a detailed examination of the Higgs boson's interactions with electroweak gauge bosons offers a powerful tool for testing the limits of the SM. Independently of the model, the most commonly used approach to describe such potential deviations is Standard Model Effective Field Theory (SMEFT). Within the SMEFT framework, Higgs-gauge boson interactions (such as $H\gamma\gamma$, $HZ\gamma$, HZZ , and HWW) are parametrically investigated via higher-dimensional operators, and deviations from SM predictions are revealed, expressing new physics effects.

Future colliders offer unique opportunities to investigate such anomalous coupling interactions. Future colliders with multi-TeV energy and high integrated luminosity make precise measurements of rare processes and multiple boson final states possible. However, lepton colliders offer significant advantages over hadron colliders, providing a clean experimental environment for studying anomalous Higgs interactions. Since leptons are elementary particles, much better control is achieved over the energy of colliding particles. Unlike hadron colliders, where large QCD backgrounds and proton remnants, lepton colliders provide well-defined initial states, virtually no pile-up, and negligible QCD activity.

We consider two types of future lepton collider: the Compact Linear Collider (CLIC) for electron-positron collision, and the Muon Collider for muon-antimuon collision. The parameters for the stage of these two colliders are as follows: $\sqrt{s} = 3$ TeV and $\mathcal{L}_{\text{int}} = 5$ ab $^{-1}$ for CLIC [3] and $\sqrt{s} = 10$ TeV and $\mathcal{L}_{\text{int}} = 10$ ab $^{-1}$ for Muon Collider [4]. Significant evaluations and research are underway regarding their construction. This study demonstrates that both colliders could be useful for investigating the effects of the anomalous Higgs interactions under consideration, focusing on examining deviations from the SM in the interactions of the Higgs boson with gauge bosons. Within the framework of the SMEFT approach, the ef-

fects of anomalous Higgs interactions are studied through processes $e^-e^+/\mu^-\mu^+ \rightarrow HZZ$ at CLIC and Muon Collider, and the sensitivity limits are evaluated. The aim is to contribute to the discovery of possible new physics signatures in the Higgs sector based on the results obtained. Recently, many studies have been conducted on the determination of Higgs boson couplings in CLIC [5–12] and Muon Collider [13–22].

II. HIGGS-GAUGE BOSON INTERACTIONS

In particle physics, the SM successfully describes fundamental particles and their interactions as a quantum field theory defined under $SU(3)_C \times SU(2)_L \times U(1)_Y$ gauge symmetry. However, the SM is insufficient for directly describing new physics effects. Therefore, the Effective Field Theory (EFT) approach is widely used to study the indirect effects of physics beyond SM. The EFT offers a model-independent framework that bridges the experimentally accessible electroweak energy scale with new physics effects expected to emerge at higher energy scales. In this approach, new physics effects are parameterized through high-dimensional operators added to the SM Lagrangian. The validity of EFT depends on the condition that the new physics scale Λ is much larger than the typical energy scale E of the process of interest ($\Lambda \gg E$). When this condition is met, the EFT offers a reliable approximation. Within the framework of SMEFT, high-dimensional operators consisting of SM fields and respecting SM gauge symmetries are used. The most dominant contributions generally come from dimension-six operators, while dimension-eight and higher operators are neglected due to their additional suppression. In this approach, lepton and baryon number conservation is ensured, and new physics effects are studied as free parameters via Wilson coefficients.

The EFT framework is particularly effective for investigating the properties and interactions of the Higgs boson in a model-independent way. In this regard, the Strongly Interacting Light Higgs (SILH) basis offers an important theoretical structure. The SILH basis assumes the Higgs boson as a pseudo-Goldstone boson arising from a strongly interacting sector and predicts that electroweak symmetry breaking occurs through this mechanism [23]. The effective Lagrangian is defined by including the four-dimensional SM Lagrangian and six-dimensional operators as follows:

$$\mathcal{L}_{\text{eff}} = \mathcal{L}_{\text{SM}} + \sum_i \bar{c}_i \mathcal{O}_i \quad (1)$$

where \mathcal{O}_i are the dimension-six operators and \bar{c}_i are the Wilson coefficients. The SILH Lagrangian with the CP-conserving operators is written below [24, 25]

$$\begin{aligned} \mathcal{L}_{\text{SILH}} = & \frac{\bar{c}_H}{2v^2} \partial^\mu (\Phi^\dagger \Phi) \partial_\mu (\Phi^\dagger \Phi) + \frac{\bar{c}_T}{2v^2} (\Phi^\dagger \overleftrightarrow{D}^\mu \Phi) (\Phi^\dagger \overleftrightarrow{D}_\mu \Phi) \\ & + \frac{ig\bar{c}_W}{m_W^2} (\Phi^\dagger T_{2k} \overleftrightarrow{D}^\mu \Phi) D^\nu W_{\mu\nu}^k + \frac{ig'\bar{c}_B}{2m_W^2} (\Phi^\dagger \overleftrightarrow{D}^\mu \Phi) \partial^\nu B_{\mu\nu} \\ & + \frac{2ig\bar{c}_{HW}}{m_W^2} (D^\mu \Phi^\dagger T_{2k} D^\nu \Phi) W_{\mu\nu}^k + \frac{ig'\bar{c}_{HB}}{m_W^2} (D^\mu \Phi^\dagger D^\nu \Phi) B_{\mu\nu} \\ & + \frac{g'^2 \bar{c}_\gamma}{m_W^2} \Phi^\dagger \Phi B_{\mu\nu} B^{\mu\nu} \end{aligned} \quad (2)$$

where v is the vacuum expectation value of the Higgs field. $T_{2k} = \sigma_k/2$, where σ_k is the Pauli matrices. $B_{\mu\nu} = \partial_\mu B_\nu - \partial_\nu B_\mu$ and $W_{\mu\nu}^k = \partial_\mu W_\nu^k - \partial_\nu W_\mu^k + g\epsilon_{ij}^k W_\mu^i W_\nu^j$ are the field strength tensors. D^μ is the covariant derivative operator with $\Phi^\dagger \overleftrightarrow{D}_\mu \Phi = \Phi^\dagger (D_\mu \Phi) - (D_\mu \Phi^\dagger) \Phi$, where Φ is the Higgs doublet in SM. The Lagrangian containing the Wilson coefficients in the SILH basis of dimension-six CP-conserving operators can be defined in terms of mass eigenstates for the $H\gamma Z$ and HZZ couplings after electroweak symmetry breaking as follows [25]:

$$\begin{aligned} \mathcal{L} = & -\frac{1}{4} g_{h\gamma\gamma} F_{\mu\nu} F^{\mu\nu} h - \frac{1}{4} g_{hzz}^{(1)} Z_{\mu\nu} Z^{\mu\nu} h - g_{hzz}^{(2)} Z_\nu \partial_\mu Z^{\mu\nu} h \\ & + \frac{1}{2} g_{hzz}^{(3)} Z_\mu Z^\mu h - \frac{1}{2} g_{h\gamma z}^{(1)} Z_{\mu\nu} F^{\mu\nu} h - g_{h\gamma z}^{(2)} Z_\nu \partial_\mu F^{\mu\nu} h \end{aligned} \quad (3)$$

where h , $F_{\mu\nu}$ and $Z_{\mu\nu}$ are the Higgs boson field, the field strength tensors of photon and Z -boson, respectively. The relationships between the Lagrangian parameters in Eq. (2) and Eq. (3) are shown below:

$$g_{h\gamma\gamma} = a_H - \frac{8g\bar{c}_\gamma s_W^2}{m_W} \quad (4)$$

$$g_{h\gamma z}^{(1)} = \frac{g s_W}{c_W m_W} [\bar{c}_{HW} - \bar{c}_{HB} + 8\bar{c}_\gamma s_W^2] \quad (5)$$

$$g_{h\gamma z}^{(2)} = \frac{g s_W}{c_W m_W} [\bar{c}_{HW} - \bar{c}_{HB} - \bar{c}_B + \bar{c}_W] \quad (6)$$

$$g_{hzz}^{(1)} = \frac{2g}{c_W^2 m_W} [\bar{c}_{HB} s_W^2 - 4\bar{c}_\gamma s_W^4 + c_W^2 \bar{c}_{HW}] \quad (7)$$

$$g_{hzz}^{(2)} = \frac{g}{c_W^2 m_W} [(\bar{c}_{HW} + \bar{c}_W) c_W^2 + (\bar{c}_B + \bar{c}_{HB}) s_W^2] \quad (8)$$

$$g_{hzz}^{(3)} = \frac{gm_W}{c_W^2} \left[1 - \frac{1}{2} \bar{c}_H - 2\bar{c}_T + 8\bar{c}_\gamma \frac{s_W^4}{c_W^2} \right] \quad (9)$$

Here, $c_W = \cos\theta_W$, $s_W = \sin\theta_W$ and θ_W is the weak mixing angle, a_H is the SM contribution at the Higgs boson to two photons vertex. As seen in Eqs. (4-9), the Higgs-gauge boson couplings in the effective Lagrangian for the anomalous $H\gamma Z$ and HZZ couplings are sensitive to the seven Wilson coefficients; \bar{c}_γ , \bar{c}_B , \bar{c}_W , \bar{c}_{HB} , \bar{c}_{HW} , \bar{c}_T , \bar{c}_H .

In this study, the effects of dimension-6 operators are investigated through Monte Carlo simulations performed with leading order using the MADGRAPH5_aMC@NLO [26] event generator. The effective Lagrangians of the SMEFT containing CP-conserving dimension-6 operators are implemented using the FeynRules [27] and UFO [28] framework. We investigate the potential of anomalous Higgs-gauge boson couplings on the process $e^-e^+ \rightarrow HZZ \rightarrow b\bar{b}l\ell\nu\bar{\nu}$ at CLIC and the process $\mu^-\mu^+ \rightarrow HZZ \rightarrow b\bar{b}l\ell\nu\bar{\nu}$ at Muon Collider.

The total cross-sections of the process $\ell^-\ell^+ \rightarrow HZZ$ at generator level as a function of coefficients \bar{c}_γ , \tilde{c}_γ , \bar{c}_{HB} , \tilde{c}_{HB} , \bar{c}_{HW} and \tilde{c}_{HW} at the CLIC and the Muon Collider are given in Fig. 1a and Fig. 1b, respectively. The total cross-sections in Fig. 1 are generated by calculating a function of the coefficient in question when all other coefficients were zero. The SM cross-section corresponds to the point $\bar{c}_\gamma = \bar{c}_{HB} = \bar{c}_{HW} = \tilde{c}_\gamma = \tilde{c}_{HB} = \tilde{c}_{HW} = 0$ in Fig. 1. The cross-sections of \bar{c}_{HB} and \bar{c}_{HW} coefficients at both colliders are seen to be larger than those of the \bar{c}_γ , \tilde{c}_γ , \tilde{c}_{HB} and \tilde{c}_{HW} coefficients. Due to the greater sensitivity of \bar{c}_{HB} and \bar{c}_{HW} coefficients compared to the others in the HZZ production process, we will focus on \bar{c}_{HB} and \bar{c}_{HW} coefficients in the following sections and as the aim of this study.

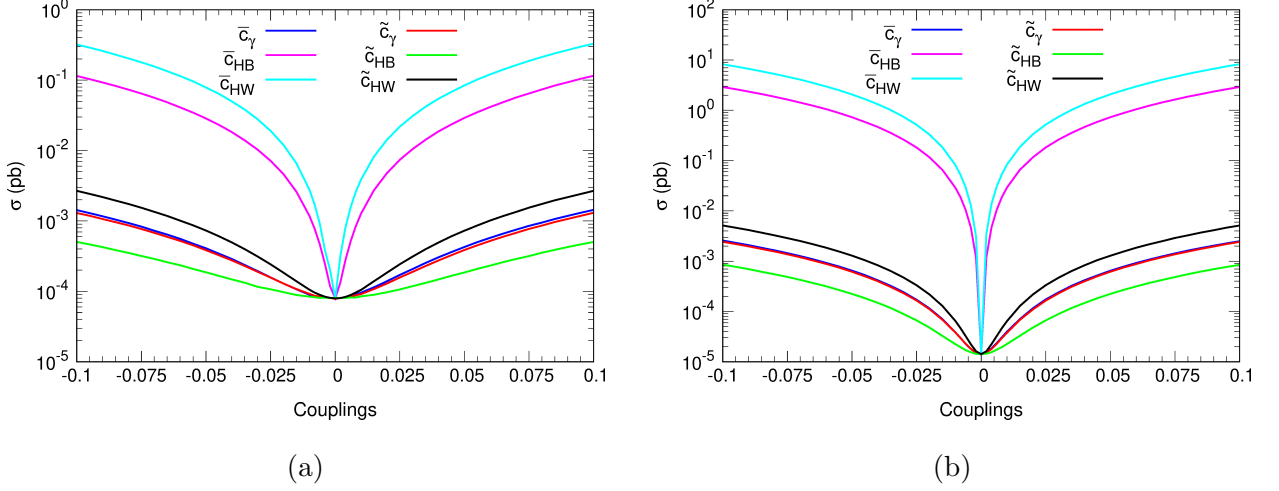


FIG. 1: The total cross-section of the process $\ell - \ell^+ \rightarrow HZZ$ as a function of coefficients \bar{c}_γ , \tilde{c}_γ , \bar{c}_{HB} , \tilde{c}_{HB} , \bar{c}_{HW} and \tilde{c}_{HW} at the CLIC (left) and the Muon Collider (right).

III. ANALYSIS OF SIGNAL AND BACKGROUND EVENTS

We present simulations and cut-based analysis to investigate the potential of HZZ production for obtaining limits on \bar{c}_{HB} and \bar{c}_{HW} coefficients of the anomalous $H\gamma Z$ and HZZ couplings within the model-independent SMEFT framework at CLIC and Muon Collider. The final state in the process $\ell^- \ell^+ \rightarrow HZZ \rightarrow b\bar{b} \ell \nu \bar{\nu}$ is formed by the decay of Higgs boson into two b quarks, and the decay of Z -bosons into charged lepton pair along with neutrino pair. A cut-based analysis is applied to enhance sensitivity by exploiting the expected signal kinematics.

We consider the following five relevant backgrounds; (i) only SM contribution from the same final state of the signal process $\ell^- \ell^+ \rightarrow HZZ \rightarrow b\bar{b} \ell \nu \bar{\nu}$, where the Higgs boson decays into two b quarks, and the Z -bosons decay into charged lepton pair along with neutrino pair; (ii) the process $\ell^- \ell^+ \rightarrow ZZZ \rightarrow b\bar{b} \ell \nu \bar{\nu}$, where the Z -bosons decay into two b quarks and charged lepton pair along with neutrino pair; (iii) the total contribution of the processes $\ell^- \ell^+ \rightarrow HWW \rightarrow b\bar{b} \ell \nu \bar{\nu}$ and $\ell^- \ell^+ \rightarrow ZWW \rightarrow b\bar{b} \ell \nu \bar{\nu}$, where W -bosons decay leptonically and H or Z -boson decay into two b quarks; (iv) the total of the contribution from the processes $\ell^- \ell^+ \rightarrow HZ \rightarrow b\bar{b} \ell \ell$ and $\ell^- \ell^+ \rightarrow ZZ \rightarrow b\bar{b} \ell \ell$, where the Z -boson decays into charged lepton pair and the H or Z -boson decay into two b quarks, and the contribution from the process $\ell^- \ell^+ \rightarrow HH \rightarrow b\bar{b}(WW/ZZ) \rightarrow b\bar{b} \ell \nu \bar{\nu}$, where one H -boson decays into

two b quarks and the other H -boson decays into $\ell\ell\nu\bar{\nu}$ via WW or ZZ production; (v) the process $\ell^-\ell^+ \rightarrow t\bar{t} \rightarrow WbW\bar{b} \rightarrow \ell\nu b\ell\bar{\nu}\bar{b}$, where W -bosons also decay leptonically as a result of t quarks decaying into Wb .

All signal and background events are generated 100k for each in MADGRAPH5_aMC@NLO and these events are processed using PYTHIA 8.3 [29] for parton showering, hadronization, fragmentation, and decay. We use Delphes 3.5.0 [30] for a fast simulation of the detector response with CLIC detector card designed for the energy stage at $\sqrt{s} = 3$ TeV and with Muon Collider detector card. In the CLIC and Muon Collider detector cards, jet clustering is performed using the Valencia Linear Collider (VLC) algorithm [31, 32] in exclusive mode with a fixed number of jets $N_j = 2$ and a cone size parameter $R = 1.0$ at $\gamma = \beta = 1$. The b-tagging efficiency is analyzed at three working points (WP) defined as the loose WP (90% b-tagging efficiency), the medium WP (70% b-tagging efficiency) and the tight WP (50% b-tagging efficiency). Misidentification rates emerge as a function of pseudo-rapidity and energy. Taking the case of $1.53 < |\eta| \leq 2.09$ and $E \geq 500$ GeV for the CLIC and Muon Collider as an example, the misidentification rates for tight WP, medium WP, and loose WP are 0.003, 0.009, and 0.05, respectively.

A. CLIC Study

The following kinematic cuts and requirements are applied to separate the signal and background at CLIC using cut-based analysis. As a pre-selection, events containing jet clustering using the VLC algorithm with $N_j = 2$, $R = 1.0$, $\gamma = \beta = 1$ and containing $N_\ell \geq 2$ same-flavour opposite-sign charged leptons are selected for further analysis (Cut-0). In the exclusive mode, two jets originating from the Higgs boson decay are identified and labeled as b-tagged jets. This selection is denoted as Cut-1. In all kinematic analyzes presented in Figs. 2-9, the b-tagging efficiency working point specified in the CLIC Delphes card is applied as the loose WP (90% b-tagging efficiency). The b-tagged jets with the highest transverse momentum (p_T) are labeled b_1 (leading), while those with the lower p_T are labeled b_2 (sub-leading). Likewise, the charged leptons are ordered by their transverse momentum, with the leading charged lepton (ℓ_1) having a higher p_T than the sub-leading charged lepton (ℓ_2). Fig. 2 shows the distributions of the transverse momentum of the leading b-tagged jet, the sub-leading b-tagged jet, the leading charged lepton, and the sub-leading charged lepton

for the signal and the relevant background processes. It is evident that the signal can be distinguished from the background by $p_T^{b_1} > 60$ GeV, $p_T^{b_2} > 20$ GeV, $p_T^{\ell_1} > 30$ GeV, $p_T^{\ell_2} > 10$ GeV. Additionally, we consider the pseudo-rapidity of the leading and sub-leading b-tagged jets ($\eta^{b_{1,2}}$), and the leading and sub-leading charged leptons ($\eta^{\ell_{1,2}}$) to be $|\eta^{b_{1,2}}| < 2.5$ and $|\eta^{\ell_{1,2}}| < 2.5$, respectively, and these are labeled Cut-2.

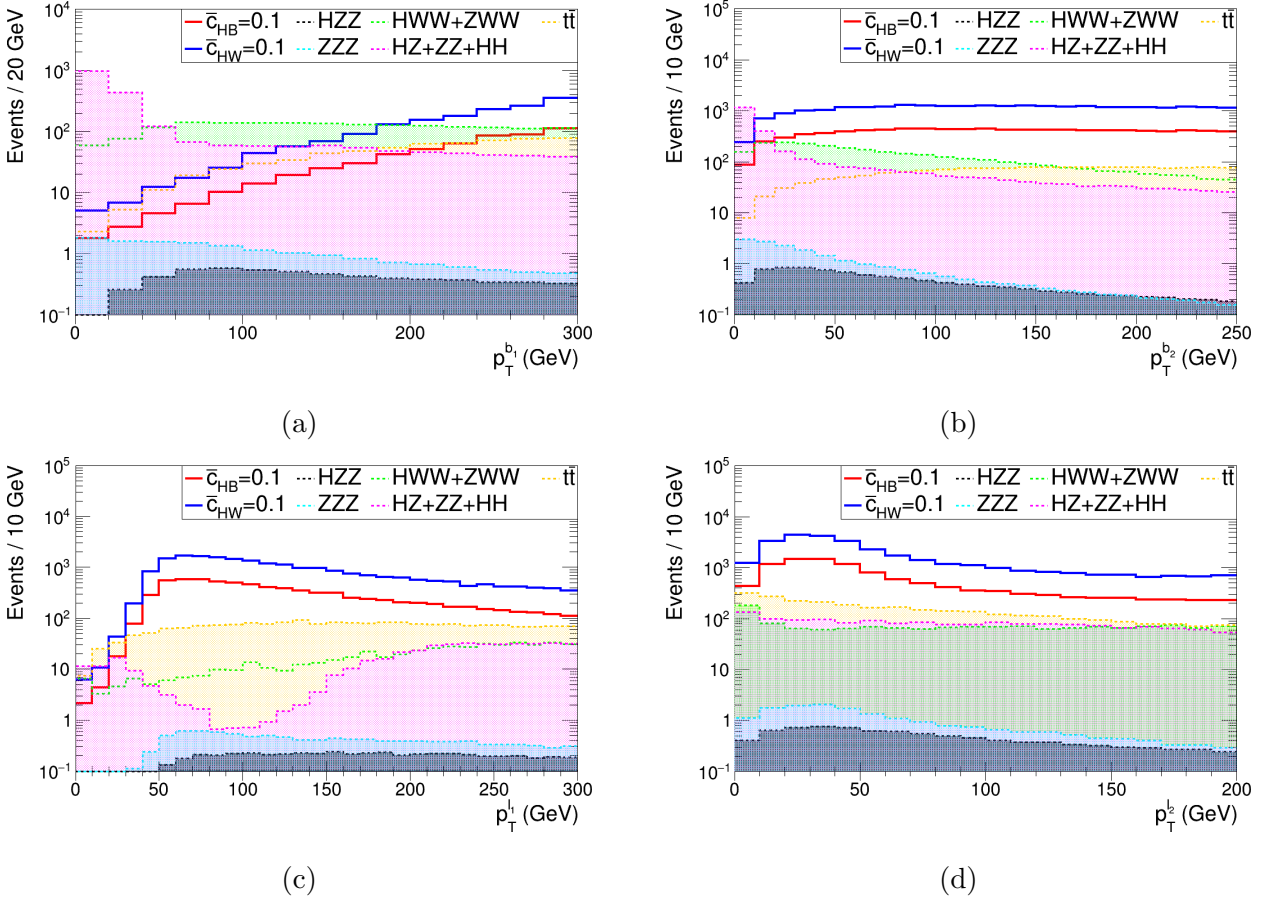


FIG. 2: The distributions of transverse momentum of the leading b-tagged jet (a), the sub-leading b-tagged jet (b), the leading charged lepton (c), and the sub-leading charged lepton (d) for signal and relevant background processes at CLIC.

The distributions of the missing energy transverse (E_T^{miss}), the transverse momentum balance ratio ($|E_T^{miss} - p_T^{\ell\ell}|/p_T^{\ell\ell}$), the scalar sum of the transverse energy (H_T), and the transverse momentum of two b-tagged jets (p_T^{bb}) for signal and background processes are shown in Fig. 3. These figures allow for the determination of the kinematic cuts: $E_T^{miss} > 50$ GeV and $|E_T^{miss} - p_T^{\ell\ell}|/p_T^{\ell\ell} > 0.5$ are labeled Cut-3 and $H_T > 200$ GeV and $p_T^{bb} > 120$ GeV are labeled Cut-4.

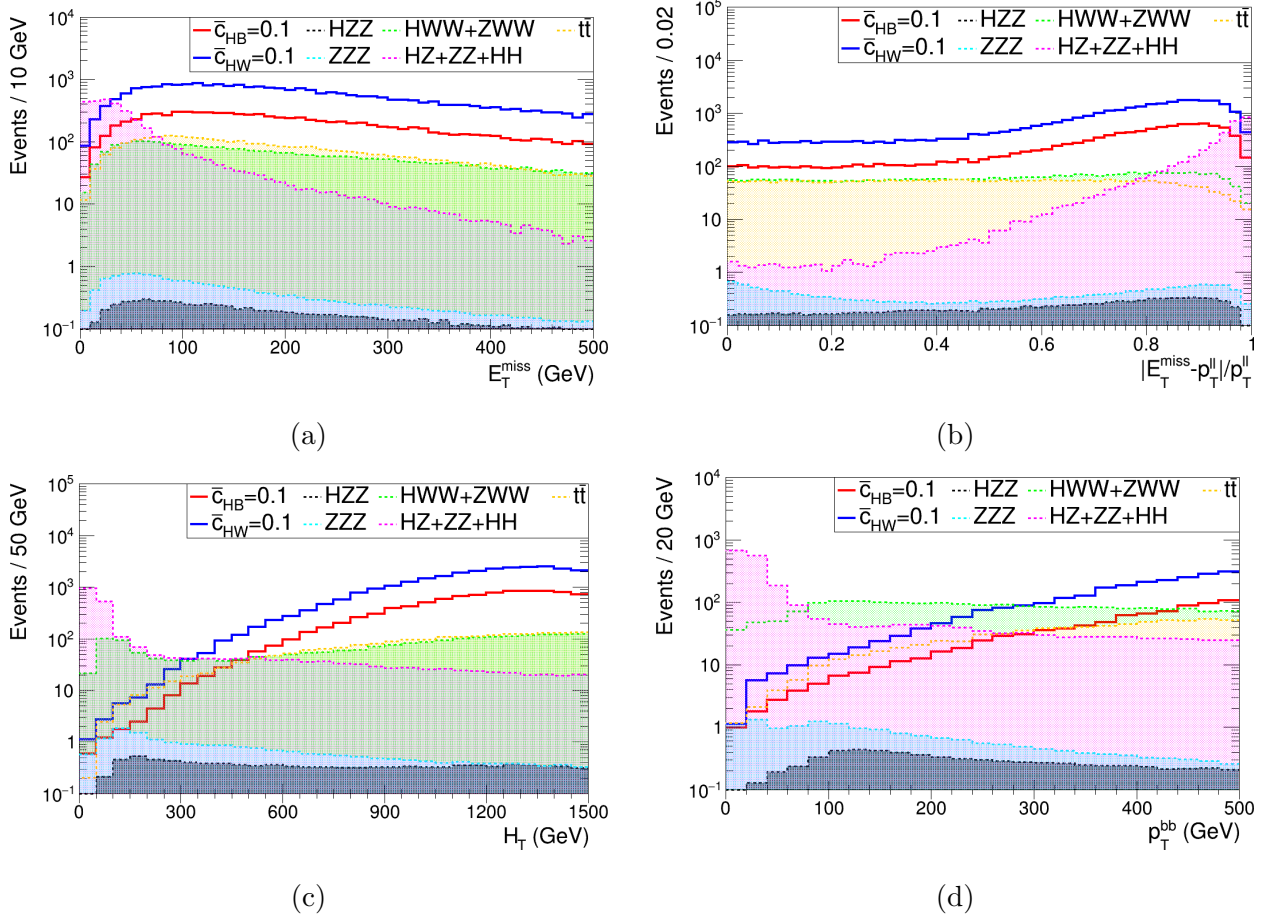


FIG. 3: The distributions of the missing energy transverse (a), the transverse momentum balance ratio (b), the scalar sum of the transverse energy (c), and the transverse momentum of two b-tagged jets (d) for signal and relevant background processes at CLIC.

In the η - ϕ space, the angular distance of two particles measured in the detector is defined as $\Delta R = \sqrt{|\Delta\eta|^2 + |\Delta\phi|^2}$, where $\Delta\eta$ and $\Delta\phi$ are differences in pseudo-rapidity and azimuthal angle, respectively. The distributions of the angular distance between the two b-tagged jets, between the two charged leptons, and between the leading charged lepton and the leading b-tagged jet are shown in Fig. 4. For the b-tagged jet and the charged lepton to be properly separated in phase space and identified as distinct objects in the detector, kinematic cuts such as $\Delta R_{bb} < 1.0$, $\Delta R_{\ell\ell} < 2.8$ and $\Delta R_{\ell b} > 0.4$ in Cut-5 are required.

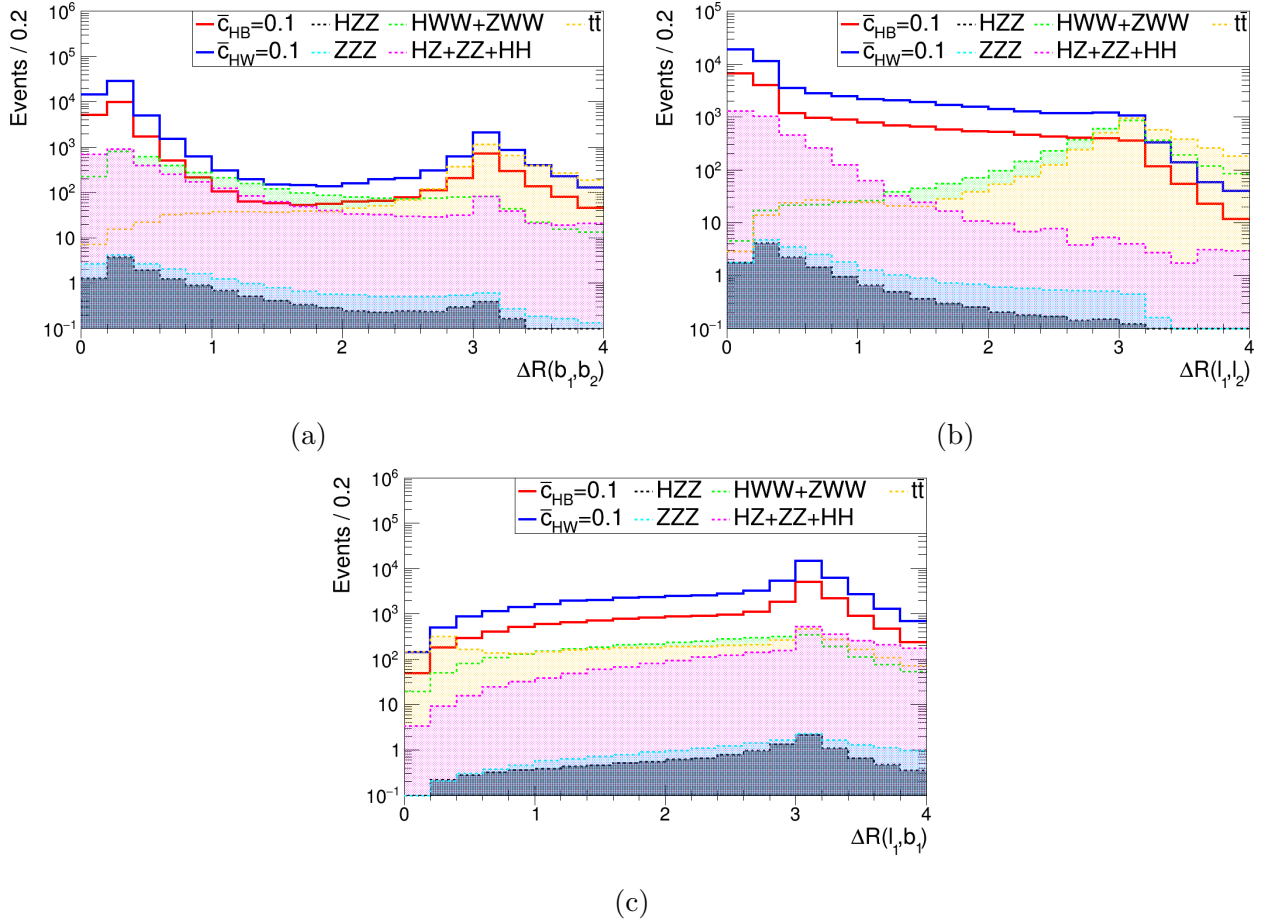


FIG. 4: The distributions of the angular distance between the two b-tagged jets (a), between the two charged leptons (b), and between the leading charged lepton and the leading b-tagged jet (c) for signal and relevant background processes at CLIC.

Guided by the invariant mass distributions of the two b-tagged jets and the charged lepton pair in Fig. 5, we set Cut-6 as $115 \text{ GeV} < m_{bb} < 135 \text{ GeV}$ and $|m_{\ell\ell} - m_Z| < 5 \text{ GeV}$, where $m_Z = 91.2 \text{ GeV}$. The b-tagging channel $H \rightarrow b\bar{b}$, which is part of the signal process, is the dominant Higgs boson decay at the LHC with a branching fraction of 53% [33]. The invariant mass of the two b-jets produced in this decay is close to 125 GeV, which is the approximate mass of the Higgs boson. As shown in Fig. 5a, the m_{bb} invariant mass distribution exhibits a clear peak around 125 GeV, which is consistent with Higgs boson production in the signal process and is essential for its experimental identification of the Higgs boson. A defined cut on the m_{bb} invariant mass will suppress the background processes $e^-e^+ \rightarrow ZZZ$, $e^-e^+ \rightarrow ZZ$, and $e^-e^+ \rightarrow ZWW$, which have a decay of $Z \rightarrow b\bar{b}$.

Since the Z -boson decays into two charged leptons in the signal process, a large number of events are observed around $m_Z \approx 91.2$ GeV according to the $m_{\ell\ell}$ invariant mass distribution in Fig. 5b. This resonance peak is a characteristic signature of an on-shell Z -boson produced in the experiment and subsequently decaying into a charged lepton pair. The determination of the $m_{\ell\ell}$ invariant mass cut around m_Z suppresses background processes that do not involve $Z \rightarrow \ell^- \ell^+$ decay, such as $e^- e^+ \rightarrow HWW$, $e^- e^+ \rightarrow ZWW$, and $e^- e^+ \rightarrow t\bar{t}$. Table I lists all the kinematic cuts used in the analysis.

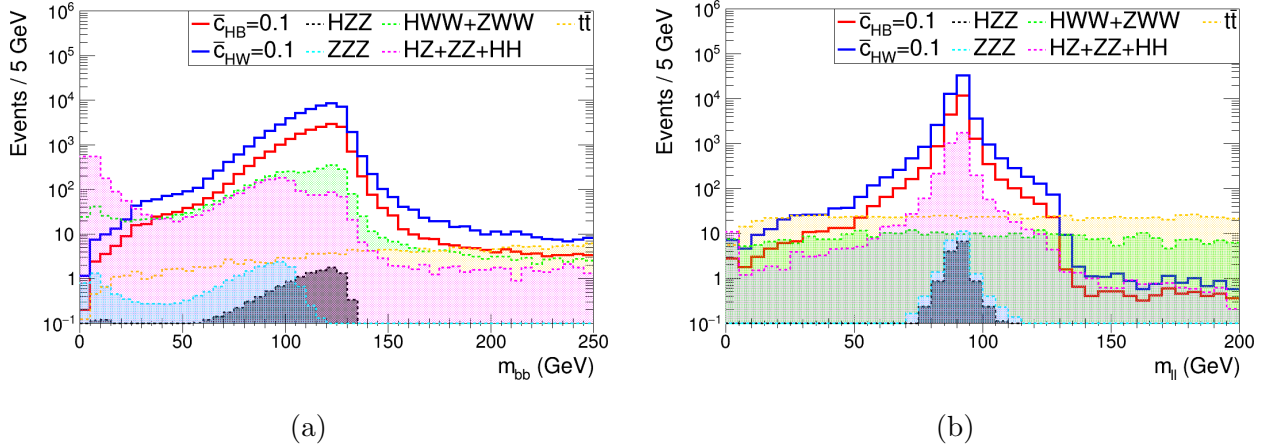


FIG. 5: The invariant mass distributions of two b-tagged jets (left) and charged lepton pair (right) for signal and relevant background processes at CLIC.

After each cut, the cumulative event numbers of the signal with setting the \bar{c}_{HB} or \bar{c}_{HW} coefficients to 0.1, respectively, and all other coefficients to zero, and of relevant backgrounds (HZZ , ZZZ , HWW , ZWW , HZ , ZZ , HH , and $t\bar{t}$) are given in Table II. In this table, the integrated luminosity of CLIC are taken into account as $\mathcal{L}_{\text{int}} = 5 \text{ ab}^{-1}$. The signal-total background ratio (S/B_{tot}) where $B_{\text{tot}} = B_{HZZ} + B_{ZZZ} + B_{HWW} + B_{ZWW} + B_{HZ} + B_{ZZ} + B_{HH} + B_{t\bar{t}}$ increases by 2362, 2017, and 1607 times for the \bar{c}_{HB} coefficient and by 2304, 1954, and 1586 times for the \bar{c}_{HW} coefficient, respectively, according to the three b-tagging efficiencies of 50%, 70%, and 90% depending on the cuts applied between Cut-0 and Cut-6, thus revealing that the applied cuts play a significant role in suppressing the relevant backgrounds.

TABLE I: Applied kinematic cuts used for the analysis at CLIC and Muon Collider.

Cut flow	CLIC at $\sqrt{s} = 3$ TeV	Muon Collider at $\sqrt{s} = 10$ TeV
Cut-0	Jet clustering: Valencia (VLC) algorithm with $R = 1.0$, $N_j = 2$ (exclusive clustering), $N_\ell \geq 2$ (least two same flavor opposite-charge leptons)	
Cut-1	two b-tagged jets	
Cut-2	$p_T^{b_1} > 60$ GeV, $p_T^{b_2} > 20$ GeV, $p_T^{\ell_1} > 30$ GeV, $p_T^{\ell_2} > 10$ GeV, $ \eta^{b_{1,2}} < 2.5$, $ \eta^{\ell_{1,2}} < 2.5$	$p_T^{b_1} > 20$ GeV, $p_T^{b_2} > 10$ GeV, $p_T^{\ell_1} > 10$ GeV, $p_T^{\ell_2} > 5$ GeV, $ \eta^{b_{1,2}} < 2.5$, $ \eta^{\ell_{1,2}} < 2.5$
Cut-3	$E_T^{miss} > 50$ GeV, p_T balance: $ E_T^{miss} - p_T^{\ell\ell} /p_T^{\ell\ell} > 0.5$	$E_T^{miss} > 10$ GeV, $ E_T^{miss} - p_T^{\ell\ell} /p_T^{\ell\ell} > 0.5$
Cut-4	$H_T > 200$ GeV, $p_T^{bb} > 120$ GeV	$H_T > 150$ GeV, $p_T^{bb} > 20$ GeV
Cut-5	$\Delta R_{bb} < 1.0$, $\Delta R_{\ell\ell} < 2.8$, $\Delta R_{\ell b} > 0.4$	$\Delta R_{bb} < 3.0$, $\Delta R_{\ell\ell} < 3.2$, $\Delta R_{\ell b} > 0.4$
Cut-6	$115 \text{ GeV} < m_{bb} < 135 \text{ GeV}$, $ m_{\ell\ell} - m_Z < 5 \text{ GeV}$	$110 \text{ GeV} < m_{bb} < 140 \text{ GeV}$, $ m_{\ell\ell} - m_Z < 5 \text{ GeV}$

TABLE II: The cumulative number of events for signal and relevant background processes at CLIC after kinematic cuts.

Cuts	b-tag.	Signals		Backgrounds				
		$\bar{c}_{HB}+B_{HZZ}$	$\bar{c}_{HW}+B_{HZZ}$	B_{HZZ}	B_{ZZZ}	$B_{HWW/ZWW}$	$B_{HZ/ZZ/HH}$	B_{tt}
Cut-0	-	8522.58	24481.9	8.21055	15.9642	1479.60	1647.71	1242.35
	50%	2027.55	5874.12	1.61615	2.39321	302.874	89.2094	197.394
Cut-1	70%	3976.47	11317.2	3.19892	4.79585	603.967	182.644	389.872
	90%	6544.17	18869.8	5.37439	8.18205	1003.22	330.449	656.993
	50%	1895.65	5498.33	1.37413	1.62431	232.583	4.77907	164.482
Cut-2	70%	3721.53	10542.0	2.72572	3.23389	464.425	9.69667	323.356
	90%	6113.11	17603.8	4.52126	5.43706	766.594	17.5579	546.309
	50%	1721.5	5004.22	0.89969	0.93892	136.648	2.18175	113.325
Cut-3	70%	3390.71	9587.00	1.78139	1.89970	270.178	4.67518	222.424
	90%	5559.78	16030.2	3.34205	2.93877	443.976	8.38069	374.513
	50%	1720.91	5004.22	0.84790	0.83723	127.741	1.76618	112.959
Cut-4	70%	3390.32	9584.18	1.67906	1.68643	252.401	3.84404	221.855
	90%	5559.00	16027.4	2.76638	2.82183	415.176	6.89156	373.253
	50%	1526.31	4397.99	0.68472	0.69642	40.5267	1.73155	0.60949
Cut-5	70%	2980.68	8385.81	1.36753	1.39769	81.3875	3.67088	1.34088
	90%	4886.95	14048.7	2.24030	2.32373	135.534	6.57988	2.43797
	50%	603.055	1689.67	0.03557	0.00230	0.09371	0	0
Cut-6	70%	1184.68	3297.64	0.07225	0.00437	0.18556	0	0.04063
	90%	1944.79	5516.92	0.10919	0.00667	0.44534	0	0.06284

B. Muon Collider Study

The pre-selection for the Muon Collider study analyses is considered the same as for the CLIC study (Cut-0). In the exclusive mode, the selection of Higgs boson decay to two jets as b-tagged jets is called Cut-1. Fig. 6 presents the transverse momentum distributions of the leading b-tagged jet, the sub-leading b-tagged jet, the leading charged lepton, and the sub-

leading charged lepton for the signal process $\mu^- \mu^+ \rightarrow HZZ$ and the relevant background processes at Muon Collider. The signal can be distinguished from the background with $p_T^{b_1} > 20$ GeV, $p_T^{b_2} > 10$ GeV, $p_T^{\ell_1} > 10$ GeV, $p_T^{\ell_2} > 5$ GeV according to this figure and furthermore, the pseudo-rapidity of the leading and sub-leading b-tagged jets ($\eta^{b_{1,2}}$), and the pseudo-rapidity of the leading and sub-leading charged leptons ($\eta^{\ell_{1,2}}$) are $|\eta^{b_{1,2}}| < 2.5$ and $|\eta^{\ell_{1,2}}| < 2.5$, respectively, which are labeled as Cut-2.

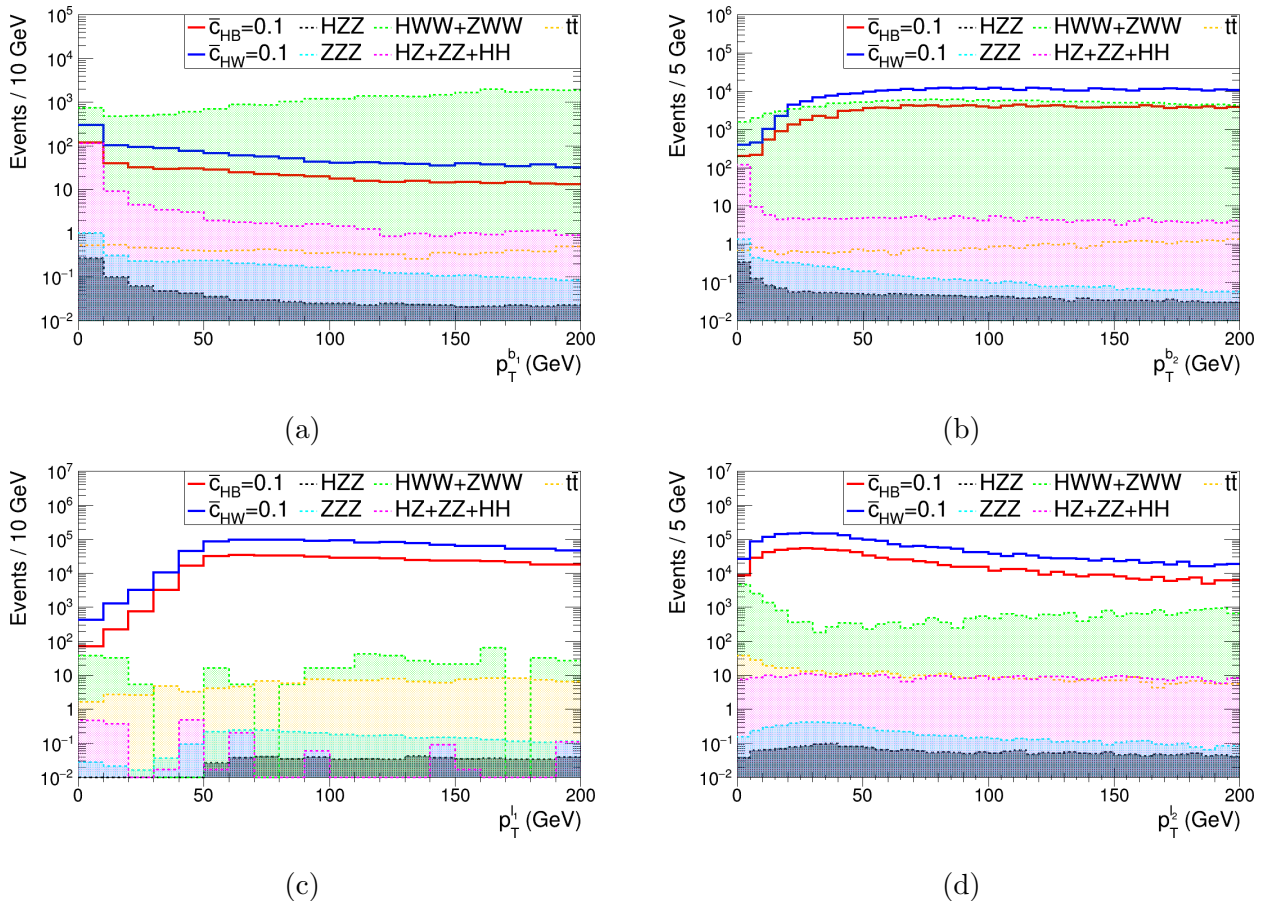


FIG. 6: The distributions of transverse momentum of the leading b-tagged jet (a), the sub-leading b-tagged jet (b), the leading charged lepton (c) and the sub-leading charged lepton (d) for signal and relevant background processes at Muon Collider.

The distributions of the missing energy transverse (E_T^{miss}), the transverse momentum balance ratio ($|E_T^{miss} - p_T^{\ell\ell}|/p_T^{\ell\ell}$), the scalar sum of the transverse energy (H_T), and the transverse momentum of two b-tagged jets (p_T^{bb}) are given in Fig. 7. We determine the kinematic cuts based on these figures: $E_T^{miss} > 10$ GeV and $|E_T^{miss} - p_T^{\ell\ell}|/p_T^{\ell\ell} > 0.5$ are labeled Cut-3 and $H_T > 150$ GeV and $p_T^{bb} > 20$ GeV are labeled Cut-4.

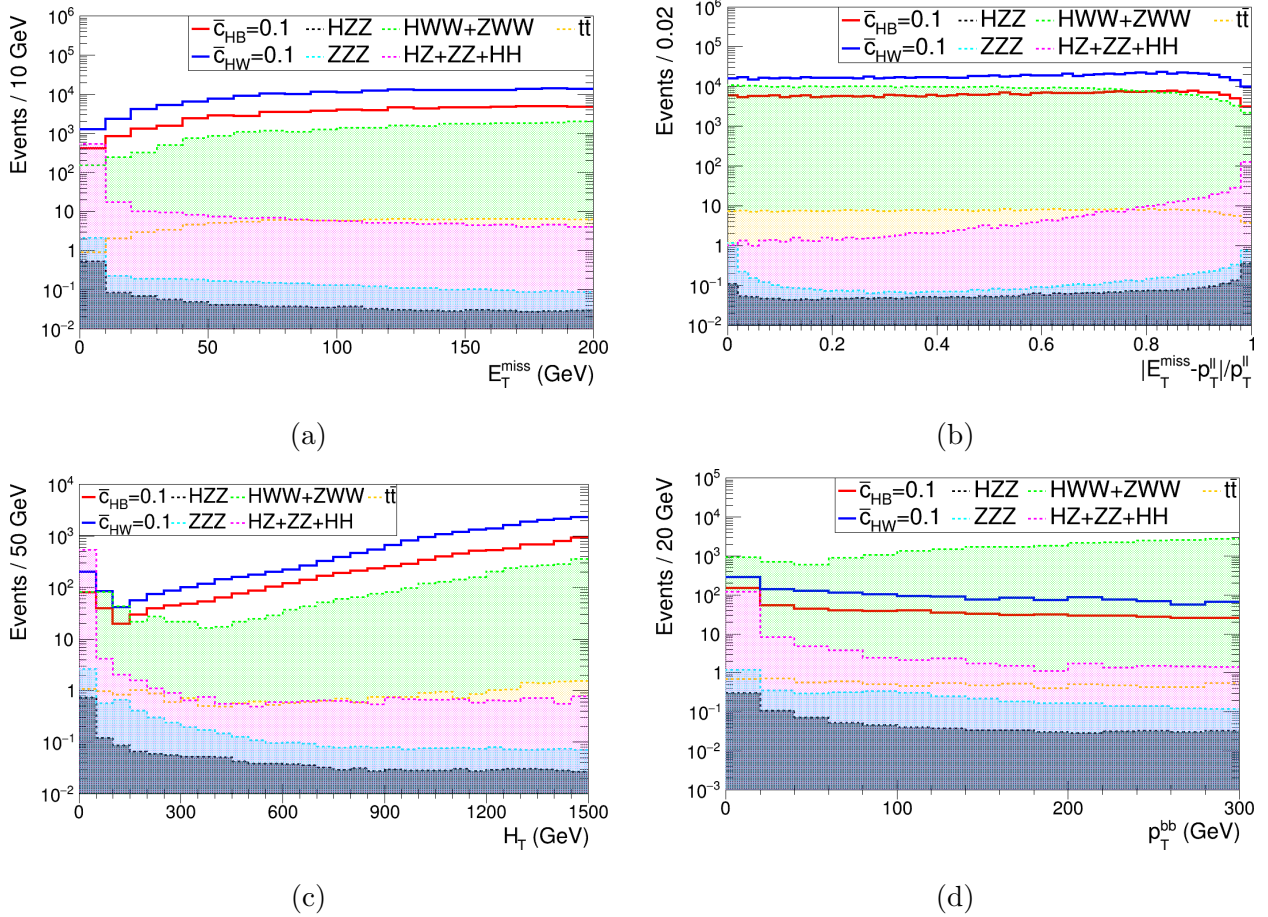


FIG. 7: The distributions of the missing energy transverse (a), the transverse momentum balance ratio (b), the scalar sum of the transverse energy (c), and the transverse momentum of two b-tagged jets (d) for signal and relevant background processes at Muon Collider.

Fig. 8 shows the distributions of the angular distance between the two b-tagged jets, between the two charged leptons, and between the leading charged lepton and the leading b-tagged jet at Muon Collider. According to these figures, kinematic cuts of $\Delta R_{bb} < 3.0$, $\Delta R_{\ell\ell} < 3.2$ and $\Delta R_{\ell b} > 0.4$ are applied in Cut-5.

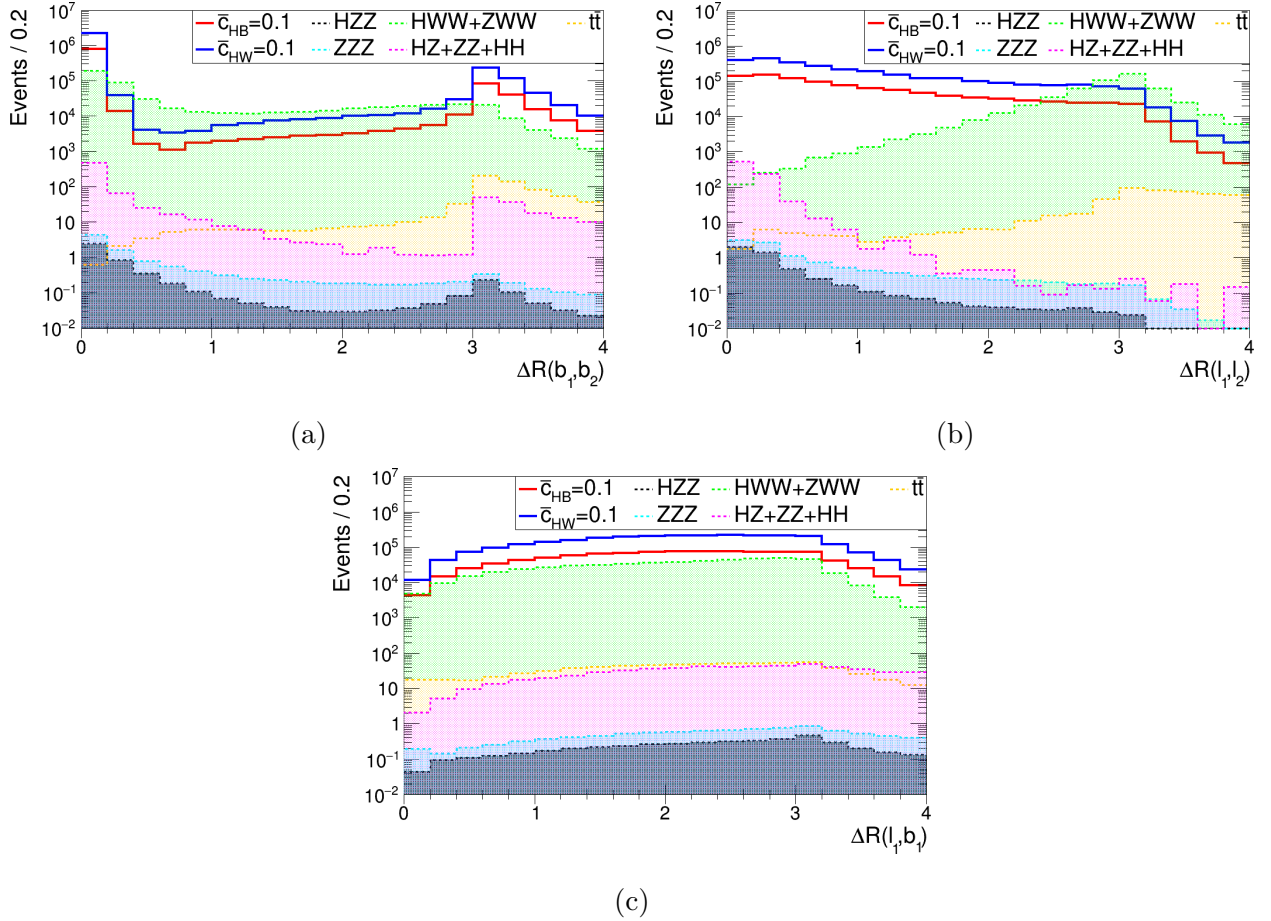


FIG. 8: The distributions of the angular distance between the two b-tagged jets (a), between the two charged leptons (b), and between the leading charged lepton and the leading b-tagged jet (c) for signal and relevant background processes at Muon Collider.

Using the invariant mass distributions of the two b-labeled jets and the charged lepton pair in Fig. 9, we defined Cut-6 as $110 \text{ GeV} < m_{bb} < 140 \text{ GeV}$ and $|m_{\ell\ell} - m_Z| < 5 \text{ GeV}$, where $m_Z = 91.2 \text{ GeV}$ to separate the signal from the backgrounds. Table I summarizes all kinematic cuts used in the analysis for the Muon Collider.

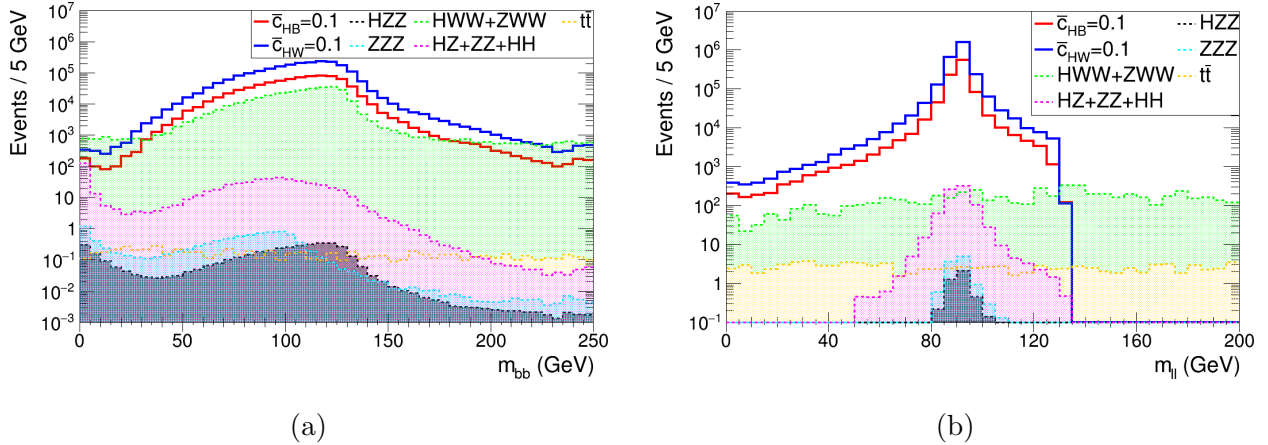


FIG. 9: The invariant mass distributions of two b-tagged jets (left) and charged lepton pair (right) for signal and relevant background processes at Muon Collider.

Table III lists the cumulative event numbers after each cut for the evaluated signal and the relevant background processes (HZZ , ZZZ , HWW , ZWW , HZ , ZZ , HH , and $t\bar{t}$), where \bar{c}_{HB} or \bar{c}_{HW} coefficient is set to 0.1 while all other parameters are fixed to zero. The results are presented assuming an integrated luminosity of $\mathcal{L}_{\text{int}} = 10 \text{ ab}^{-1}$ for Muon Collider. As kinematic cuts from Cut-0 to Cut-6 are applied, the signal-total-background ratio (S/B_{tot}), where $B_{\text{tot}} = B_{HZZ} + B_{ZZZ} + B_{HWW} + B_{ZWW} + B_{HZ} + B_{ZZ} + B_{HH} + B_{t\bar{t}}$, improves by factors of 1638, 1664, and 1616 for \bar{c}_{HB} coefficient, and by 1633, 1641, and 1593 for \bar{c}_{HW} coefficient, respectively, according to the three b-tagging efficiencies of 50%, 70%, and 90%. These results clearly demonstrate the effectiveness of the applied cuts in reducing the background contributions.

TABLE III: The cumulative number of events for signal and relevant background processes at Muon Collider after kinematic cuts.

Cuts	b-tag.	Signals		Backgrounds				
		$\bar{c}_{HB}+B_{HZZ}$	$\bar{c}_{HW}+B_{HZZ}$	B_{HZZ}	B_{ZZZ}	$B_{HWW/ZWW}$	$B_{HZ/ZZ/HH}$	B_{tt}
Cut-0	-	886751	2523920	4.01960	9.62668	230208	284.470	307.096
	50%	185185	523669	0.78993	1.73920	40420.3	35.2828	55.0737
Cut-1	70%	363376	1028180	1.55496	3.39546	78448.5	72.9413	107.953
	90%	604579	1718830	2.61650	5.71429	130389	126.885	185.411
	50%	183637	518442	0.74772	1.59560	39583.1	28.8357	51.0738
Cut-2	70%	360172	1018290	1.47015	3.11957	76817.5	59.7701	99.7036
	90%	598865	1702660	2.45649	5.18106	127448	100.610	171.202
	50%	161784	457952	0.50932	0.87362	22224.4	9.57832	40.4172
Cut-3	70%	317011	896608	1.00597	1.73015	42344.8	19.9122	79.7408
	90%	526896	1496730	1.67272	2.88498	70859.2	33.6374	136.429
	50%	161774	457924	0.46905	0.71292	22213.5	8.33591	40.4025
Cut-4	70%	316981	896579	0.93041	1.40130	42323.0	17.7463	79.7041
	90%	526886	1496730	1.54561	2.33150	70804.8	29.9774	136.363
	50%	156913	443628	0.44892	0.68780	16896.6	8.06728	0.88070
Cut-5	70%	306773	867140	0.89014	1.34879	32347.1	16.9069	1.83481
	90%	508524	1441780	1.46732	2.23350	54125.7	28.3488	4.24208
	50%	54896.8	155872	0.01963	0.00497	8.40621	0.29381	0
Cut-6	70%	107314	301148	0.04150	0.01018	16.3095	0.41973	0
	90%	178459	500586	0.06700	0.01708	27.8807	0.77231	0

IV. SENSITIVITIES ON THE HIGGS-GAUGE BOSON COUPLINGS

The χ^2 test is used to calculate the sensitivity of dimension-six Higgs-gauge boson couplings in the process $\ell^-\ell^+ \rightarrow HZZ$. The analysis utilizes the χ^2 distribution to determine limits at 95% Confidence Level (C.L.) with a threshold value of 3.84 for one degree of freedom. The χ^2 distribution is defined as follows:

$$\chi^2 = \sum_i^{n_{bins}} \left(\frac{N_i^{NP} - N_i^B}{N_i^B \Delta_i} \right)^2 \quad (10)$$

where by integrating the invariant mass $m_{\ell\ell b\bar{b}}$ distribution of $\ell\ell b\bar{b}$ system after Cut-6, N_i^B is the number of events of relevant total backgrounds in i th bin and N_i^{NP} is the total number of events including contributions of effective couplings and relevant total backgrounds in i th bin. $\Delta_i = \sqrt{1/N_i^B}$ is the statistical uncertainty in each bin.

Fig. 10 shows the four-body invariant mass distributions of the two leptons and two b-jets system after Cut-0 (left) and after Cut-6 (right) for the signal and relevant background processes at CLIC (top) and Muon Collider (bottom).

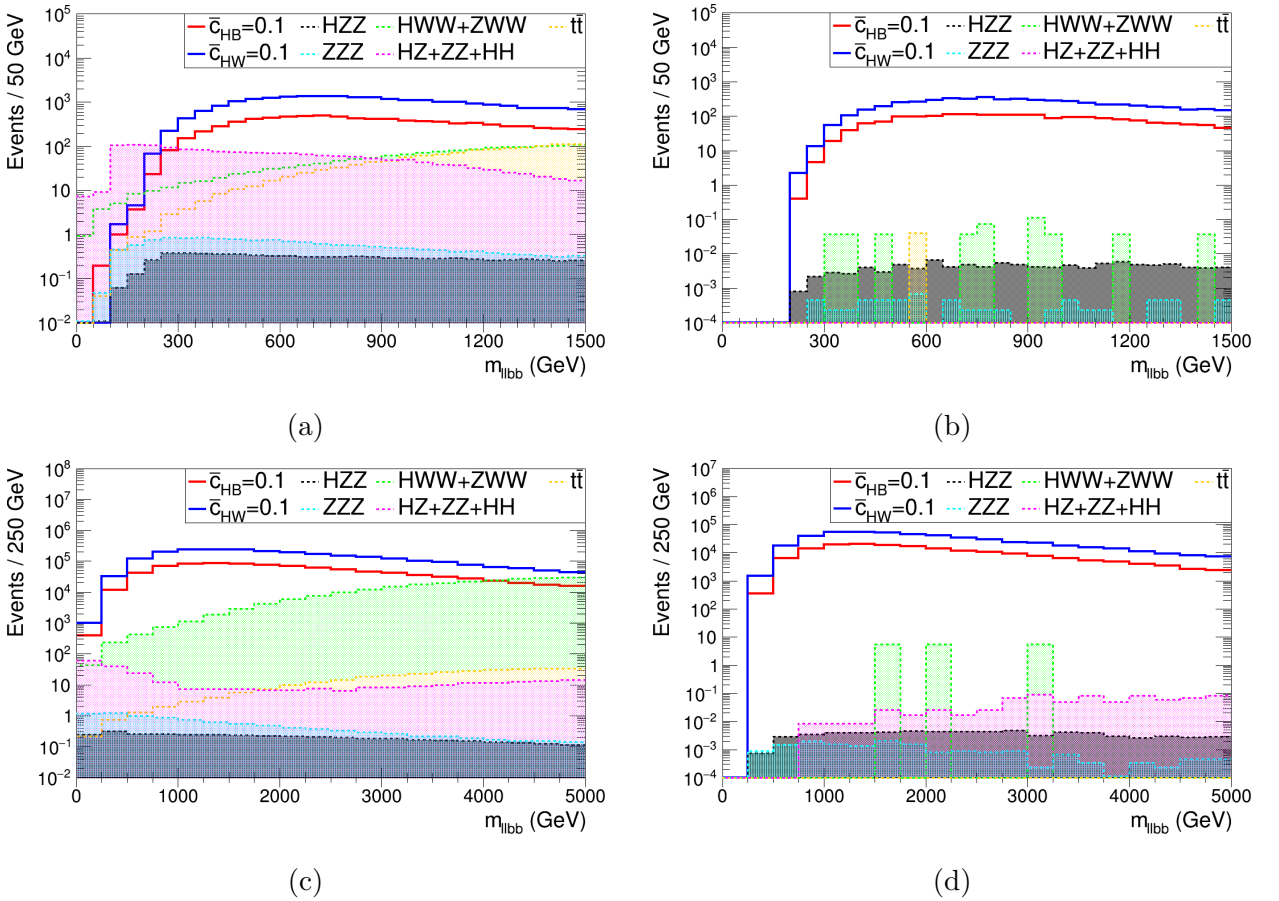


FIG. 10: The invariant mass distributions of the two leptons and two b-jets system after Cut-0 (left) and after Cut-6 (right) for the signal and relevant background processes at CLIC (top) and Muon Collider (bottom).

In this study, we focus on obtaining the 95% C.L. limits of \bar{c}_{HB} and \bar{c}_{HW} coefficients

through the $\ell^-\ell^+ \rightarrow HZZ$ signal process with a stage at $\sqrt{s} = 3$ TeV and $\mathcal{L}_{\text{int}} = 5$ ab $^{-1}$ for CLIC and a stage at $\sqrt{s} = 10$ TeV and $\mathcal{L}_{\text{int}} = 10$ ab $^{-1}$ for Muon Collider. The 95% C.L. limits of \bar{c}_{HB} and \bar{c}_{HW} coefficients, including detector effects, are given in Table IV using the one-parameter analysis. Since $H \rightarrow b\bar{b}$ is the decay channel in the final state of the signal process, b-tagging efficiency has a significant role in the analysis. This effect is demonstrated in Table IV through a comparison of b-tagging efficiencies for CLIC and Muon Collider at three working points. According to the results in the table, it is emphasized that the sensitivity of the limits for CLIC and Muon Collider increases with increasing b-tagging efficiency, and a better limit is reached with the loose working point (90% b-tagging efficiency). Furthermore, comparing the limits of recent experimental and previous phenomenological studies with our own limits, as shown in Table IV, is one of the notable aims of our study. A detailed comparison of the limits in Table IV will be presented in Section V.

TABLE IV: The 95% C.L. limits on \bar{c}_{HB} and \bar{c}_{HW} coefficients in various experimental and phenomenological studies, and in our study.

Coefficients		\bar{c}_{HB}	\bar{c}_{HW}	
Experimental Results (ATLAS)		[−0.057; 0.051] [34]	[−0.057; 0.051] [34]	
		[−0.090; 0.032] [35]	[−0.005; 0.006] [35]	
		[−0.025; 0.022] [36]	[−0.025; 0.022] [36]	
Phenomenological Results		[−0.004; 0.004] [37]	[−0.004; 0.004] [37]	
		[−0.0172; 0.00661] [38]	[−0.00187; 0.0018] [38]	
		–	[−0.0032; 0.0035] [39]	
		[−0.230; 0.236] [40]	[−0.236; 0.231] [40]	
		[−0.39; 0.41] [41]	[−0.18; 0.17] [41]	
		[−0.0482; 0.0153] [7]	[−0.00658; 0.00555] [7]	
		[−2.5608; 1.3256] [11]	[−0.7692; 0.3969] [11]	
<u>This study</u>	<u>b-tag.</u>			
	50%	[−0.00156; 0.00182]	[−0.00187; 0.00035]	
	3 TeV CLIC	70%	[−0.00124; 0.00082]	[−0.00175; 0.00021]
		90%	[−0.00098; 0.00047]	[−0.00158; 0.00008]
		50%	[−0.00023; 0.00023]	[−0.00021; 0.00009]
	10 TeV Muon Collider	70%	[−0.00022; 0.00021]	[−0.00020; 0.00008]
90%		[−0.00021; 0.00019]	[−0.00019; 0.00007]	

The 95% C.L. contour for examining the relationship between the two coefficients in the $\bar{c}_{HB} - \bar{c}_{HW}$ plane at CLIC and Muon Collider using two-parameter analysis is given in Fig. 11. Furthermore, in Fig. 11, the contours in both colliders are evaluated for 50% and 90% b-tagging efficiencies, and it is determined that a narrower contour is formed with 90% b-tagging efficiency. In this analysis, the 95% C.L. contour is obtained with a χ^2 value of 5.99 corresponding to two degrees of freedom.

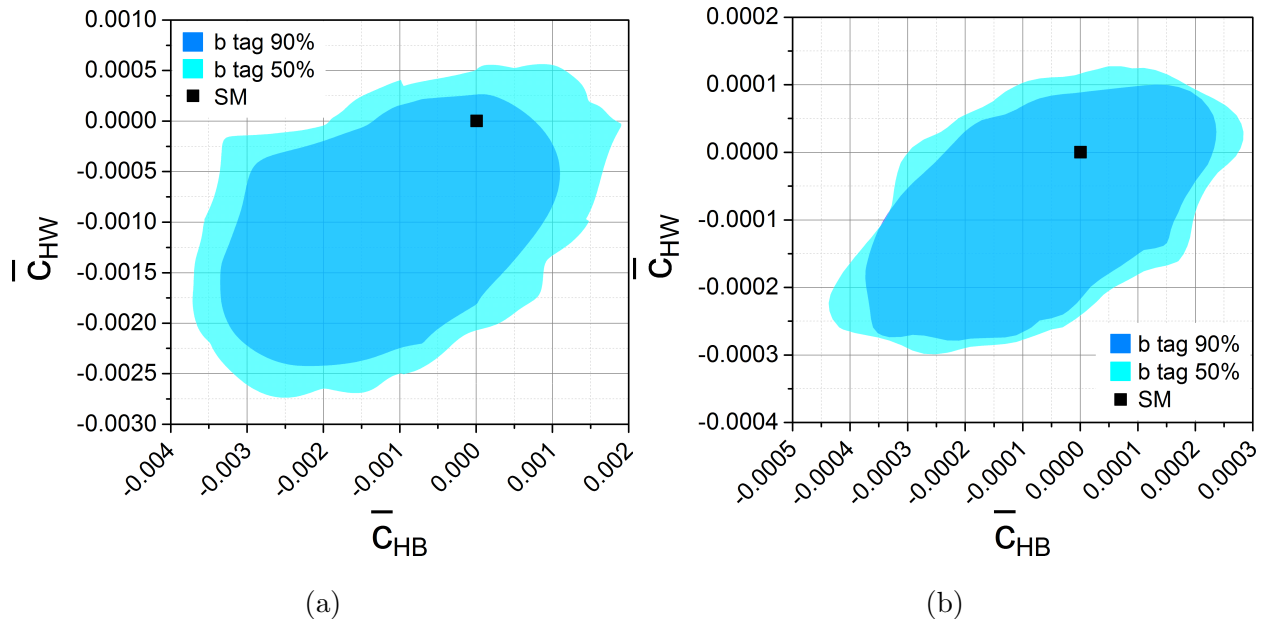


FIG. 11: Two-dimensional 95% C.L. intervals in $\bar{c}_{HB} - \bar{c}_{HW}$ plane at CLIC (left) and Muon Collider (right).

V. CONCLUSIONS

Among future colliders, CLIC and Muon Collider are attractive options recently due to their multi-TeV energies and clean environments for exploring Higgs interactions in new physics beyond the SM. We investigate the dimension-six operators of Higgs-gauge boson couplings $H\gamma Z$ and HZZ via the process $\ell^-\ell^+ \rightarrow HZZ$ at CLIC and Muon Collider using an effective Lagrangian approximation in the SILH basis. We analyze the production of $bb\ell\ell\nu\nu$ final state along with the decay of H and Z -bosons, considering the realistic detector effects. We present the kinematic distributions of the signal and relevant background processes using cut-based analysis to separate signal events from backgrounds. The 95% C.L. limits on the Wilson coefficients \bar{c}_{HB} and \bar{c}_{HW} in the SILH basis are obtained using the χ^2 test from the invariant mass distribution of the $\ell\ell bb$ system for three working points of b-tagging efficiency. The best limits in our study are obtained at the loose working point (90% b-tagging efficiency); these are $[-0.00098; 0.00047]$ for the coefficient \bar{c}_{HB} and $[-0.00158; 0.00008]$ for the coefficient \bar{c}_{HW} at CLIC, and $[-0.00021; 0.00019]$ for the coefficient \bar{c}_{HB} and $[-0.00019; 0.00007]$ for the coefficient \bar{c}_{HW} at Muon Collider.

In Table IV, we present a comparison between the 95% C.L. limits of the \bar{c}_{HB} and \bar{c}_{HW} co-

efficients from this study and those reported in various phenomenological and experimental studies. First, let us consider the comparison of the sensitivities of \bar{c}_{HB} and \bar{c}_{HW} coefficients at CLIC and Muon Collider in this study with experimental studies. Among the experimental studies, the most sensitive limit at 95% C.L. for the coefficient \bar{c}_{HW} was determined by ATLAS collaboration [35] as $[-0.005; 0.006]$ at $\sqrt{s} = 13$ TeV with $\mathcal{L}_{\text{int}} = 79.8 \text{ fb}^{-1}$, and the most sensitive limit at 95% C.L. for the coefficient \bar{c}_{HB} was obtained by ATLAS collaboration [36] as $[-0.025; 0.022]$ at $\sqrt{s} = 13$ TeV with $\mathcal{L}_{\text{int}} = 139 \text{ fb}^{-1}$. The 95% C.L. limits of \bar{c}_{HB} coefficient at CLIC and Muon Collider in our study are approximately 32 times and 118 times more sensitive than the limit in Ref. [36], respectively, and the 95% C.L. limits of \bar{c}_{HW} coefficient at CLIC and Muon Collider are approximately 7 times and 42 times more sensitive than the limit in Ref. [35], respectively.

Table IV presents the limits of some phenomenological studies involving different processes and decay channels at LHC [37, 40], FCC-he [39], ILC [38, 41], CLIC [7], and Muon Collider [11, 21]. The most sensitive limit for the coefficient \bar{c}_{HB} was given as $[-0.004; 0.004]$ in Ref. [37] performed at LHC with $\sqrt{s} = 14$ TeV and $\mathcal{L}_{\text{int}} = 3000 \text{ fb}^{-1}$. The most sensitive limit for the coefficient \bar{c}_{HW} was obtained as $[-0.00187; 0.0018]$ in Ref. [38] performed at an electron-positron collider with $\sqrt{s} = 350$ GeV and $\mathcal{L}_{\text{int}} = 3000 \text{ fb}^{-1}$. In our study, the 95% C.L. limits of the \bar{c}_{HB} coefficient at CLIC and Muon Collider are approximately 6 times and 20 times more sensitive than the limit in Ref. [37], respectively. The 95% C.L. limits of the \bar{c}_{HW} coefficient at CLIC and Muon Collider are approximately 2 times and 14 times more sensitive than the limit in Ref. [38], respectively.

The clean experimental environment of the future lepton colliders, with their high center-of-mass energy and integrated luminosity, presents a very promising option for testing the SM predictions and searching new physics beyond the SM. The fact that the limits on \bar{c}_{HB} and \bar{c}_{HW} coefficients for anomalous $H\gamma Z$ and HZZ couplings at CLIC and Muon Collider are more sensitive than those from experimental studies at LHC highlights the potential of CLIC and Muon Collider. The study of Higgs physics will be greatly enriched by the combined insights from future lepton colliders and supplementary measurements from hadron colliders. The results certainly encourage a more detailed and comprehensive investigation of lepton colliders.

Declaration of competing interest

The authors declare that they have no known competing financial interests or personal relationships that could have appeared to influence the work reported in this paper.

- [1] G. Aad *et al.* [ATLAS Collaboration], *Phys. Lett. B* **716**, 1-29 (2012).
- [2] S. Chatrchyan *et al.* [CMS Collaboration], *Phys. Lett. B* **716**, 30-61 (2012).
- [3] A. Robson and P. Roloff, “Updated CLIC luminosity staging baseline and Higgs coupling prospects,” (2018) [arXiv:1812.01644 [hep-ex]].
- [4] C. Aime *et al.* [International Muon Collider Collaboration], “Muon Collider Physics Summary,” (2022) [arXiv:2203.07256 [hep-ph]].
- [5] H. Abramowicz *et al.*, *Eur. Phys. J. C* **77**, 475 (2017).
- [6] J. Ellis, P. Roloff, V. Sanz and T. You, *JHEP* **05**, 096 (2017).
- [7] H. Denizli and A. Senol, *Adv. High Energy Phys.* **2018**, 1627051 (2018).
- [8] B. Sahin, *Mod. Phys. Lett. A* **34**, 1950299 (2019).
- [9] O. Karadeniz, A. Senol, K. Y. Oyulmaz and H. Denizli, *Eur. Phys. J. C* **80**, 229 (2020).
- [10] P. Roloff, U. Schnoor, R. Simoniello and B. Xu, *Eur. Phys. J. C* **80**, 1010 (2020).
- [11] S. Spor, *J. Phys. G: Nucl. Part. Phys.* **51**, 065003 (2024).
- [12] C. H. de Lima and D. Tuckler, *Phys. Rev. D* **111**, 015021 (2025).
- [13] M. Chiesa, F. Maltoni, L. Mantani, B. Mele, F. Piccinini and X. Zhao, *JHEP* **09**, 098 (2020).
- [14] T. Han, D. Liu, I. Low and X. Wang, *Phys. Rev. D* **103**, 013002 (2021).
- [15] J. Chen, C-T. Lu and Y. Wu, *JHEP* **10**, 099 (2021).
- [16] T. Han, W. Kilian, N. Kreher, Y. Ma, J. Reuter, T. Striegl and K. Xie, *JHEP* **12**, 162 (2021).
- [17] J. Chen, T. Li, C-T. Lu, Y. Wu and C-Y. Yao, *Phys. Rev. D* **105**, 053009 (2022).
- [18] M. Forsslund and P. Meade, *JHEP* **08**, 185 (2022).
- [19] J. de Blas, J. Gu and Z. Liu, *Phys. Rev. D* **106**, 073007 (2022).
- [20] S. Spor and E. Gurkanli, “Analysis of anomalous $H\gamma\gamma$ coupling in light-by-light collision at future muon collider,” (2024) [arXiv:2412.02346 [hep-ph]].
- [21] S. Spor, *Nucl. Phys. B* **1020**, 117170 (2025).
- [22] E. Gurkanli and S. Spor, *PTEP* **2025**, 053B05 (2025).

- [23] C. Tosciri, Theoretical Introduction. *In: Higgs Boson Decays into a Pair of Bottom Quarks*, Springer, 2021.
- [24] G. F. Giudice, C. Grojean, A. Pomarol and R. Rattazzi, *JHEP* **06**, 045 (2007).
- [25] A. Alloul, B. Fuks and V. Sanz, *JHEP* **04**, 110 (2014).
- [26] J. Alwall, R. Frederix, S. Frixione, V. Hirschi, F. Maltoni, O. Mattelaer, H. S. Shao, T. Stelzer, P. Torrielli and M. Zaro, *JHEP* **07**, 079 (2014).
- [27] A. Alloul, N. D. Christensen, C. Degrande, C. Duhr and B. Fuks, *Comput. Phys. Commun.* **185**, 2250-2300 (2014).
- [28] C. Degrande, C. Duhr, B. Fuks, D. Grellscheid, O. Mattelaer and T. Reiter, *Comput. Phys. Commun.* **183**, 1201-1214 (2012).
- [29] C. Bierlich *et al.*, *SciPost Phys. Codebases* **8** (2022).
- [30] J. de Favereau, C. Delaere, P. Demin, A. Giammanco, V. Lemaitre, A. Mertens and M. Selvaggi [DELPHES 3 Collaboration], *JHEP* **02**, 057 (2014).
- [31] M. Boronat, J. Fuster, I. García, E. Ros and M. Vos, *Phys. Lett. B* **750**, 95-99 (2015).
- [32] M. Boronat, J. Fuster, I. Garcia, P. Roloff, R. Simoniello and M. Vos, *Eur. Phys. J. C* **78**, 144 (2018).
- [33] S. Navas *et al.* [Particle Data Group], *Phys. Rev. D* **110**, 030001 (2024).
- [34] M. Aaboud *et al.* [ATLAS Collaboration], *Phys. Rev. D* **98**, 052005 (2018).
- [35] M. Aaboud *et al.* [ATLAS Collaboration], *JHEP* **05**, 141 (2019).
- [36] ATLAS Collaboration, “Measurements and interpretations of Higgs-boson fiducial cross sections in the diphoton decay channel using 139 fb⁻¹ of *pp* collision data at $\sqrt{s} = 13$ TeV with the ATLAS detector,” ATLAS-CONF-2019-029 (2019).
- [37] C. Englert, R. Kogler, H. Schulz and M. Spannowsky, *Eur. Phys. J. C* **76**, 393 (2016).
- [38] H. Khanpour and M. M. Najafabadi, *Phys. Rev. D* **95**, 055026 (2017).
- [39] H. Hesari, H. Khanpour and M. M. Najafabadi, *Phys. Rev. D* **97**, 095041 (2018).
- [40] L. Shi, Z. Liang, B. Liu and Z. He, *Chin. Phys. C* **43**, 043001 (2019).
- [41] S. Kumar, P. Poulse, R. Rahaman and R. K. Singh, *Int. J. Mod. Phys. A* **34**, 1950094 (2019).